Improved thermal management in HKUST-1 composites upon graphite flakes incorporation: Hydrogen adsorption properties

Judit Farrando-Pérez [a], María Rodríguez-Castillo [b],
Manuel Martínez-Escandell [a], Miguel Monge [b], Joaquin Silvestre-Albero [a,*]

[a] Laboratorio de Materiales Avanzados, Departamento de Química Inorgánica-Instituto Universitario de Materiales, Universidad de Alicante, San Vicente del Raspeig, 03690, Spain
[b] Departamento de Química, Centro de Investigaciones en Síntesis Química (CSIQ), Universidad de La Rioja, Complejo Científico- Tecnológico, Logroño, 26006, Spain

HIGHLIGHTS

- Thermal events in metal-organic frameworks (e.g., HKUST-1) can be modulated through the incorporation of graphite flakes.
- The presence of GF in the composites improves the mechanical stability of HKUST-1 upon a conforming step.
- HKUST-1@GF monoliths possess excellent adsorption properties for hydrogen at cryogenic temperatures.

GRAPHICAL ABSTRACT
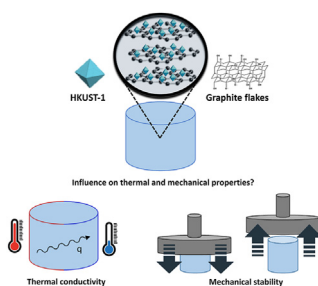
ARTICLE INFO

ABSTRACT

HKUST-1-based composites have been synthesized through the incorporation of synthetic graphite flakes in the MOF synthesis media. The presence of flakes gives rise to high quality HKUST-1 crystals, combining different morphologies (octahedral-shape crystals, cauliflower-shape crystals and truncated pyramids). The incorporation of graphite in the composites improves the structural stability of the embedded nanocrystals upon a conforming step at 377 kg/cm² (0.5 tons), with limited structural damage (below 10% BET surface area reduction as compared to the 40% observed for pure HKUST-1). Furthermore, composites exhibit a significant improvement in thermal management, associated with the excellent thermal and electrical properties of the graphite microdomains incorporated. The improved stability of the composites is also reflected in the adsorption performance for hydrogen at atmospheric pressure and cryogenic temperatures, with a significant preservation of the adsorption properties (gravimetric capacity, <15% decrease vs powders) in the monoliths containing graphite. The best adsorption performance is achieved with

sample HKUST-1@10GF, in monolithic form, with a volumetric excess uptake at 0.1 MPa and −195 °C close to 18.7 g/L. This value is among the best described in the literature for monolithic MOFs under similar adsorption conditions.

Introduction

Recent changes in global weather patterns and the increase number of natural disasters worldwide is raising up the societal concern towards climate change and the necessity to find renewable and less contaminant energy sources [1]. Among the different possibilities, hydrogen is emerging as a promising energy vector for mobile and stationary devices through the well-known fuel cell technology [2]. One of the critical aspects in the hydrogen technology is the necessity to design proper storage devices able to concentrate a large amount of hydrogen in a minimum volume [3]. In this sense, concentration of hydrogen in the cavities of nanoporous materials is a very promising approach to reach high storage values at medium pressures and cryogenic temperatures. This is, for instance, the case of metal-organic frameworks (MOFs) combining a proper porous structure and surface chemistry [4]. Using properly designed MOFs, hydrogen storage values around 5−10 wt% have been easily reached at high pressures (~10 MPa) and low temperatures (−195 °C) [4,5]. Unfortunately, these gravimetric values are precluded by the low density of the powder samples, thus given rise to volumetric values below 10 g/L under high-pressure conditions [6]. Densification of metal-organic frameworks can be achieved through a mechanical compaction. However, these conforming processes are traditionally associated with a significant deterioration of the porous network through plastic deformation and/or amorphization [7]. Recent studies from Tian [8] and Connelly [9] et al. have anticipated that MOFs densification can also be achieved through a sol-gel approach, minimizing the instability issues associated with the conventional conforming approach. HKUST-1 monoliths synthesized using the sol-gel approach can adsorb up to 24 g/L at atmospheric pressure and cryogenic temperatures and up to 45 g/L at higher pressures [10].

Despite the excellent results achieved so far in terms of gravimetric and volumetric capacity, a critical issue not widely evaluated in the MOF field is the thermal management upon adsorption. Gas adsorption is an exothermic process and the heat generated during the adsorption step must be immediately dissipated to avoid large thermal spikes in the adsorption bed. A similar scenario occurs during the desorption step due to the endothermic nature of the process. These thermal events are even more critical for large-scale storage beds and fast refueling (e.g., storage tanks for mobile applications) with temperature spikes around 40−70 °C or above (for instance, for methane) [11,12]. The presence of a widely developed porous structure and large intergranular spaces infers to MOFs a thermal insulator character, with thermal conductivities below 2 W m^{-1} K^{-1} [13]. Thermal management in MOFs is not an easy task due to the large phonon scattering in voids and cavities, and the detrimental effect of remaining and/or adsorbed molecules as secondary scattering centers [13]. These limitations have been minimized through the incorporation of expanded natural graphite (ENG) in the MOF formulation [6,14]. Using this approach, Liu et al. managed to improve the thermal conductivity of MOF-5 in monolithic form in a factor of five (up to 0.56 W m^{-1} K^{-1}), although at the expenses of a lower gravimetric adsorption capacity [14]. Although the newly developed monoliths had a higher thermal conductivity than the MOF single crystal (0.32 W m^{-1} K^{-1}), the obtained values are still too small for a practical application, similarly to the hydrogen adsorption values (3−4 wt%) [15]. HKUST-1 constitutes another example of a promising MOF for hydrogen storage (up to 20 g/L at 2 MPa), but associated with a low thermal conductivity (single crystal conductivity *ca.* 0.69 W m^{-1} K^{-1}) and a low mechanical stability upon mechanical compaction [7,13]. Previous studies from some of us have anticipated that structural properties of HKUST-1 and the associated adsorption properties can be highly improved through the nucleation and growth of HKUST-1 crystals in the nanocavities of high surface area activated carbon materials [16]. Despite these excellent findings, to our knowledge there are no studies in the literature dealing with the modification of the thermal properties of HKUST-1 using thermal modifiers, while trying to preserve their excellent adsorption performance. Based on these premises, the main goal of the present study is the modification of the thermal properties of HKUST-1 crystals through the incorporation of high conductivity graphite flakes (GF) in the synthesis media. To get a clear overview of the structural, mechanical and thermal properties of the composites (HKUST-1@xGF), in powder and monolithic shape, different compositions have been evaluated from pure MOF to samples with x = 10 wt%, 25 wt%, 50 wt% GF and pure GF. The synthesized monoliths have also been evaluated in the adsorption of hydrogen at atmospheric pressure and cryogenic temperatures. The obtained values (*ca.* 19 g/L at 0.1 MPa) are among the best described in the literature for hydrogen storage in monoliths, with the additional advantages of improved thermal and mechanical properties.

Materials and methods

Materials

High conductivity synthetic graphite flakes with anisometric particle shape (TIMREX®SFG150) were supplied by Imerys Graphite & Carbon Ltd. Trimesic acid (C$_6$H$_3$(CO$_2$H)$_3$, Benzene-

1,3,5-tricarboxylic acid, BTC), was purchased from Sigma Aldrich Corporation. Copper nitrate hydrate ($Cu(NO_3)_2 \cdot 3H_2O$) was purchased from Panreac Quimica SA and Ethanol (CH_3-CH_2OH, 96%) was purchased from VWR International.

Synthesis of the composites in monolithic and powder form

Pure HKUST-1 and HKUST-1 based composite materials have been prepared using a modified hydrothermal method, based on recipes already reported in the literature [17,18].

For HKUST-1, 0.84 g of BTC (BTC = 1,3,5-benzenetricarboxylate) were dissolved in 24 mL of ethanol. In a separated flask, 1.75 g of $Cu(NO_3)_2 \cdot 3H_2O$ were dissolved in 24 mL of ultrapure water. The BTC solution was slowly added to the copper solution and maintained under stirring for 30 min at room temperature. The resulting solution was transferred into a 100 mL Teflon-lined autoclave and cooked at 110 °C for 18 h. After allowing the autoclave and its contents to cool down to room temperature, a blue crystalline solid was collected and washed with ethanol several times. Finally, the sample was dried at 80 °C for 12 h.

The same procedure was used to synthesize HKUST-1 based composite materials (named HKUST-1@xGF), but adding different amounts of graphite flakes 15 min after mixing the linker and metal solutions. More specifically, 0.13 g, 0.38 g and 1.15 g of graphite flakes (TIMREX®SFG150) were added to obtained composites with 10 wt% (HKUST-1@10GF), 25 wt% (HKUST-1@25GF) and 50 wt% (HKUST-1@50GF) graphite flakes.

The different powders synthesized, i.e. HKUST-1, HKUST-1@10GF, HKUST-1@25GF, HKUST-1@50GF and pure graphite flakes were conformed into disk-shaped monoliths under a load of 0.5 Tons (corresponding pressure 40 MPa or 377 kg/m^3 after considering the cross-sectional area of the monolith (ca. 1.32 cm^2)).

Physicochemical characterization of the synthesized composites

The textural characteristics of the synthesized composites (powder or monoliths) were evaluated using nitrogen adsorption at cryogenic temperatures (−195 °C). Gas adsorption measurements were performed in a home-built fully automated manometric equipment designed and developed by the LMA (Advanced Materials Lab) group at the University of Alicante. Prior to the adsorption measurements, samples were outgassed at 150 °C for 12 h under ultra-high vacuum conditions. Specific surface area was obtained after application of the BET equation to the nitrogen adsorption data. In the specific case of the monoliths, samples were crashed and sieved down to 3−4 mm, to fit the adsorption reactor.

The crystallographic quality of the synthesized composites was evaluated using X-ray diffraction (XRD). XRD patterns were recorded using a Bruker D8-Advance instrument equipped with a Goebel mirror and a high temperature chamber. X-rays are generated in a KRISTALLOFLEX K tube equipped with a copper anode. X-ray photoelectron spectroscopy (XPS) measurements were performed in a k-Alpha spectrometer from Thermo-Scientific. Thermogravimetric experiments were obtained in a Mettler Toledo TGA/SDTA instrument. To obtain the thermograms, an alumina crucible containing

10 mg of sample was heated up to 975 °C under an air flow of 100 mL/min (heating rate 10 °C/min). Thermal conductivity of the synthesized monoliths was evaluated using a thermal analyzer C-Therm TCi from Mathis Instruments ltd. based on the modified transient plane source (MTPS) principle. Before performing the thermal conductivity measurements, samples were heat treated at 150 °C for additional 12 h to remove adsorbed species and minimize alterations in the conductivity values. Electrical conductivity values were performed under similar conditions using a Keithley 2700 multimeter.

The compressive strength measurements were performed in a 5 KN Instron Universal testing machine model 4411, using parallel plates. The tests were performed at a 0.1 mm/min deformation rate using cylindrical samples of 1.3 cm diameter and 2 mm height. Compressive modulus was calculated from the slope of the stress/strain curve in the linear region. Compressive strength was determined as the maximum value of stress in the stress/strain curve before the failure of the sample.

The photothermal heating of the samples was performed using a MDL−III−808 R NIR laser working with an 808 nm wavelength and 0.6 W cm^{-2} irradiation power. The thermal heating of the samples was carried out using a LLG-uniSTIRRER 7-inch ceramic hotplate heater for sample heating and a similar ceramic plate at room temperature for sample cooling. For all the experiments, the temperature increase and sample cooling were monitored using a FLIR E6-XT thermographic camera and the images were treated with the FLIR Tools software. Video files were built up using time-monitored thermographic images using the software VSDC video editor.

Hydrogen adsorption measurements

The synthesized samples in powder and monolith shape have been evaluated in the adsorption of hydrogen at cryogenic temperatures (−195.8 °C) and up to atmospheric pressure. Prior to the adsorption measurements, samples were outgassed at 150 °C for 12 h under ultra-high vacuum conditions (monoliths were crashed and sieved).

Results and discussion

Structural and chemical characterization of the powder composites

It is well-known in the literature that morphological characteristics of metal-organic frameworks (size and shape of the crystals) can be modified in the presence of secondary species incorporated in the synthesis media or when electrodeposited in supports [19,20]. To identify the potential interference of graphite flakes (GF) in the nucleation and growth of the MOF crystals, X-ray diffraction measurements have been performed in the synthesized powder composites. Fig. 1 shows that all samples exhibit the characteristic peaks of the parent MOF with maxima at 6.7°, 9.5°, 11.6°, 13.4° and 19.1°, corresponding to (200), (220), (222), (400) and (440) diffraction peaks, respectively [21]. The intensity of the main diffraction peaks is rather similar among composites, and similar to that of the parent
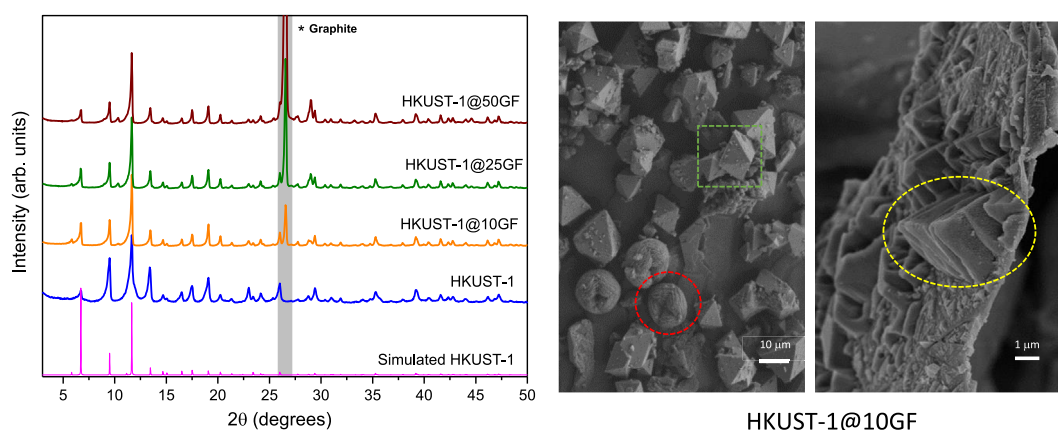
Fig. 1 — (Right) X-ray diffraction pattern of the synthesized composites (HKUST-1@xGF) in powder form and (left) representative FE-SEM images of the composite material with 10 wt% GF.

MOF (XRD pattern for all samples has been normalized to the intensity of the (222) peak). These observations confirm the high quality of the HKUST-1 crystals grown in the composites, despite the presence of graphite flakes. XRD pattern of the composites also reflect the main peak of graphite (002) at 26.5°.

The high quality of the synthesized crystals has been confirmed with FE-SEM images. Original HKUST-1 crystals show the typical octahedral shape with crystal sizes in the micrometer range (*ca.* 10 μm) (Fig. S1) [21]. Incorporation of graphite flakes in the synthesis media gives rise to a similar growth patterns, independently of the MOF@GF ratio selected. Three different growth patterns can be observed for all composites (Fig. 1), i.e. octahedral crystal grown on the graphite substrate (dotted square), cauliflower-shape morphology (dotted circles), and truncated pyramids grown on the basal planes of the graphite flakes (dotted ovals). These results confirm the success in the synthesis of HKUST-1 crystals in the presence of a graphite flakes and the effect of the carbon media in the morphology of the resulting MOFs.

The textural characteristics of the synthesized samples have been characterized by nitrogen adsorption at cryogenic temperatures. Results in Fig. S2 show that the original MOF in powder form exhibits the highest porosity, with a BET surface area of 1330 m^2/g, and a micropore volume of 0.5 cm^3/g (Table S1). On the contrary, graphite flakes are non-porous, with a BET surface area close to zero. Composite materials exhibit an intermediate performance. Incorporation of a small amount of graphite (10 wt% GF) does not infer appreciable changes in the textural properties, i.e. surface area and micropore volume are rather similar to pure MOF. Larger contents of graphite flakes (25 wt% and 50 wt%) become detrimental for the textural properties due to the null contribution from the flakes. BET surface area of the composites ranges from 1327 m^2/g down to 734 m^2/g, for the lowest and largest GF content, respectively. However, the normalization of the nitrogen adsorption isotherms to the amount of HKUST-1 incorporated shows a relatively similar performance for the pure MOF and the composites, thus confirming the success in the synthesis of HKUST-1 in the presence of graphite.

An open question at this step concerns the quantification of the amount of MOF grown in each of the formulations

evaluated, as compared to the nominal value. To this end, the thermogravimetric performance of the different composites and the raw materials has been evaluated in an air atmosphere in the temperature range from 25 °C and up to 975 °C. As it can be appreciated in Fig. 2, the thermal performance of the different composites differs considerable from their parent components. Graphite flakes exhibit a high thermal stability in an oxidizing atmosphere up to 700 °C [22]. Above this temperature, graphite burns in a small temperature window (700—950 °C), with no residues formed (complete combustion). On the contrary, HKUST-1 exhibits an initial weight loss at 100—200 °C due to the removal of moisture and remaining solvent. Above 280 °C, HKUST-1 exhibits a sudden weight decrease due to the decomposition of the MOF, the final residual weight being *ca.* 30 wt% (due to the reaction $Cu_3(BTC)_2 \rightarrow CuO$) [23]. Interestingly, the composites exhibit a more complex thermogravimetric profile. In addition to the removal of humidity/solvent below 280 °C, composites exhibit two well-defined losses at 280 °C and 600 °C. The first step corresponds to the decomposition of the MOF, in close agreement with the results in the pure MOF, while the second
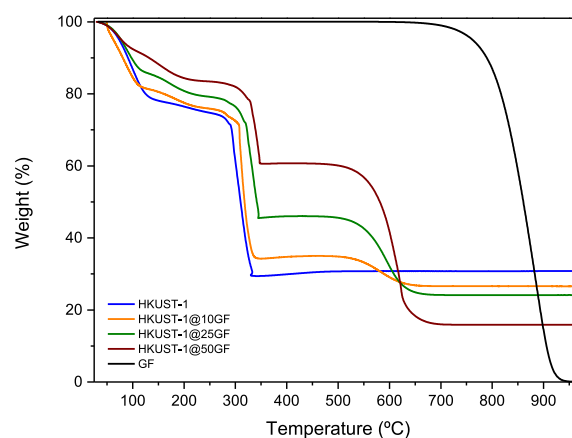
Fig. 2 — Thermogravimetric analysis of the evaluated composites under an air atmosphere and in the temperature range 25 °C up to 975 °C.

step at higher temperatures correspond, unambiguously, to the oxidation/combustion of the graphite flakes promoted by CuO nanoparticles from the decomposed MOF. These results constitute another confirmation about the synergetic effects between the graphite substrate and the supported MOF nanocrystals. After proper correction of humidity, the weight loss associated with graphite corresponds to 11%, 27% and 54% weight percent, values that are rather close to the nominal content. The residual mass at 975 °C due to remaining CuO increases with the amount of MOF in the composite, ranging from 30.8 wt% (original HKUST-1) down to 26.6, 24.1 and 15.9 wt%, for samples HKUST-1@xGF, x = 10, 25 and 50, respectively.

The chemical composition of the original samples and the composites has been evaluated using X-ray photoelectron spectroscopy analysis (XPS). As expected, the original MOF and the composites are composed of Cu, C, O and N (Table S2). In general, the atomic percentage of these elements decrease after the incorporation of graphite, except the carbon content that increases. The estimated Cu/C ratio progressively decreases with the GF content in the composites, in agreement with the thermogravimetric measurements.

Packing and mechanical properties of the monoliths

Upon characterization of the synthesized composites in powder form, samples were compacted into monoliths using a conforming pressure of 0.5 tons, i.e. 377 kg/cm^2. For a constant mass of composites (0.3 g), the monoliths were prepared in a pellet die hydraulic machine (Specac) using stain-steel wafers with a cross-sectional area of 1.32 cm^2. The height of the monoliths differs depending on the density of the final composite, ranging from 2.01 mm (pure HKUST-1), 2.07 mm (10GF), 1.98 mm (25GF), 1.61 mm (50GF) and 1.27 mm (pure GF) for

pure components and composites, respectively. The density of the monoliths was estimated using two different approaches. In a first approach, a given amount of sample was incorporated in the powder pressing mold and the compaction process was performed using a mechanical testing machine with precise control of the applied pressure and the bed height. Packing density over the whole process (under pressure) has been estimated from the height and the amount of sample incorporated. Fig. 3 shows that the packing density under pressure highly depends on the sample evaluated. The density is higher for graphite flakes with a density at 38 MPa of ca. 2.30 g/cm^3, a value very close to the crystallographic density of graphene and graphite (Table 1) [24]. The density of the composites under pressure is rather similar among them (ca. 1.7–1.8 g/cm^3), although some divergencies are appreciated for samples HKUST-1@50GF (1.98 g/cm^3) and HKUST-1@10GF (1.40 g/cm^3). The higher density of the HKUST-1@50GF composite is clearly associated with the large content in high density graphite. However, the performance of the HKUST-1@10GF sample, with a lower density than the original MOF is, a priori, unexpected. This behavior could be explained by the interference effect of graphite flakes in the packing of the MOF nanocrystals. In the second approach, the packing density has been measured upon releasing the applied pressure, i.e. from the geometric dimensions of the obtained monoliths (star symbols in Fig. 3). Although the last value is the real density of the monoliths, the comparison between both columns in Table 1 provides information about the swelling of the monoliths when releasing the pressure. Interestingly, the release of the applied pressure gives rise to an expansion of the monoliths (decrease in the packing density), independently of their composition. As expected, the swelling is much larger for graphite. In close agreement with the dynamic tests, the geometric packing density is larger for GF (1.73 g/cm^3),
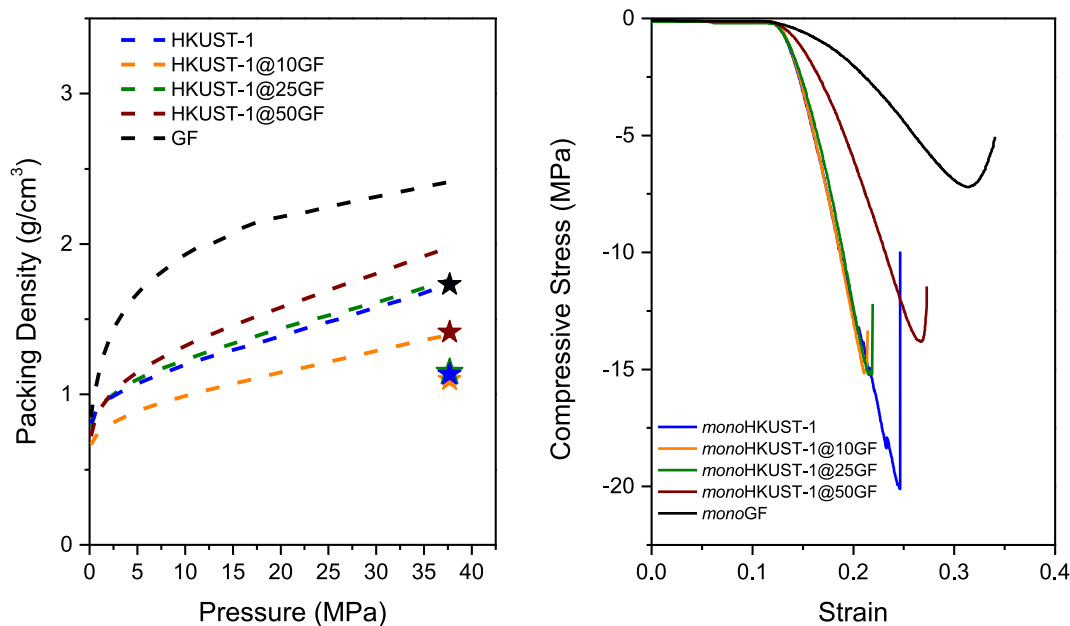
Fig. 3 – (Left) Variation of the packing density for the different composites, including the pure HKUST-1 and GF, as a function of the applied pressure (MPa). The real packing density upon releasing the pressure has been included as a star. (Right) Compressive stress (MPa) – strain tests in the different monoliths.

Table 1 – Packing density and mechanical properties for the different monoliths evaluated (experimental errors at 95% confidence are included).

| Sample	Packing properties		Mechanical properties	
	Packing density (g/cm^3)	Packing density under pressure (g/cm^3)	Compressive strength at failure (MPa)	Compressive modulus (MPa)
HKUST-1	1.13 ± 0.05	1.74 ± 0.05	20 ± 0.5	190 ± 5
HKUST-1@10GF	1.10 ± 0.05	1.40 ± 0.05	15.2 ± 0.5	200 ± 5
HKUST-1@25GF	1.15 ± 0.05	1.76 ± 0.05	15 ± 0.5	201 ± 5
HKUST-1@50GF	1.41 ± 0.05	1.98 ± 0.05	13.8 ± 0.5	125 ± 5
GF	1.73 ± 0.05	2.30 ± 0.05	7.2 ± 0.5	51 ± 5

followed by sample HKUST-1@50GF (1.41 g/cm^3). The composites with a lower GF content resemble the pure MOF with a packing density around 1.13 g/cm^3. The monolithic density achieved is very similar to the density of *mono*HKUST-1 samples prepared through the sol-gel approach [10].

Incorporation of graphite flakes in the composites could be detrimental for the mechanical properties and the integrity of the monoliths due to the different morphology of the carbon and MOF grains and the absence of a linker. Upon the conforming step, the compressibility performance of the monoliths was tested using an automated mechanical testing machine (Fig. S3). Experimental results show that the original HKUST-1 monoliths exhibit an extraordinary performance with a high compressive modulus and a high compressive strength at failure even in the absence of a binder (Fig. 3 and Table 1). In other words, HKUST-1 nanocrystals exhibit self-sintering ability giving rise to highly robust monoliths. Incorporation of 10 wt% and 25 wt% graphite flakes does not alter significantly these extraordinary properties, with compressive modulus close to 200 MPa. Larger GF contents (above 25 wt%) become detrimental for the mechanical properties of the

composites with significant losses in the compressive modulus and strength.

Textural properties of the monoliths

Another critical aspect in the conformation of some MOFs concerns the limited structural stability of the inner porous structure under mechanical stress. HKUST-1 constitutes a typical example, with a poor mechanical stability even after a low-pressure mechanical conformation [7]. The structural stability of the synthesized composites has been evaluated through nitrogen adsorption isotherms before and after the conforming step (see experimental information for further details). Fig. 4 compares the performance of the original HKUST-1 sample with the performance of the composites with (a) 10 wt%, (b) 25 wt%, and (c) 50 wt% GF. As anticipated in the literature, a conforming pressure of ca. 377 kg/cm^2 becomes detrimental for the pure MOF with a decrease in the adsorption capacity close to 45%. This observation confirms the limited stability of 3D network in HKUST-1 upon pressure. Contrariwise, the incorporation of graphite flakes gives rise to
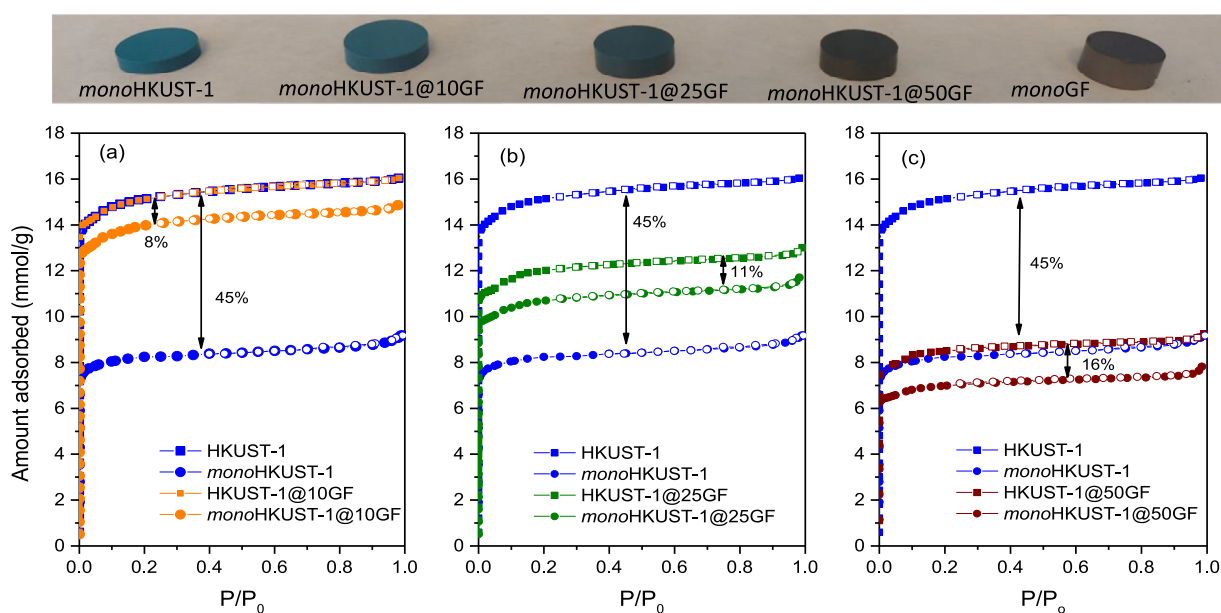
Fig. 4 – N$_2$ adsorption/desorption isotherms at cryogenic temperatures (−195 °C) for the different samples evaluated, before (powders) and after a confirming stress at 377 kg/cm^2 (monoliths).

a significant improvement in the structural stability of the encapsulated MOF crystals. Independently of the amount of graphite incorporated, the structural deterioration upon pressure ranges from 8% (for sample HKUST-1@10GF), down to 16% (for sample HKUST-1@50GF). In other words, these results confirm that the incorporation of only 10 wt% GF in the formulation is sufficient to largely preserve the structural integrity of HKUST-1 after a conforming step, thus giving rise to highly stable and robust (e.g., mechanical properties in Fig. 3) monoliths.

The improved structural stability of the composites is also reflected in the textural parameters (Table S1). BET surface area and micropore volume confirm the beneficial effect of only 10 wt% GF in the preservation of the 3D microporous network of the parent MOF upon a conforming step.

Thermal and electrical properties of the monoliths

Thermal management in gas storage tanks is a key issue for scale-up and implementation [25,26]. Tanks filled with porous solids suffer from sharp thermal spikes during refueling due to the exothermic nature of the dynamic adsorption process in a short timescale (fast filling). Consequently, materials able to extract this heat from the tank in a fast and reliable way are needed to mitigate the drawbacks associated with thermal events [27]. Recent studies from Grande et al. have shown that thermal effects in a gas storage tank filled with activated carbon as a sorbent can give rise to a temperature increase around 70 °C when dosing methane at 4 MPa [12]. The extraction of the heat generated in the adsorption bed is mandatory to preserve the adsorption capacity of the sorbent, i.e., thermodynamics decrease physisorption capacity at high adsorption temperatures. Previous studies described in the literature have anticipated that the addition of expanded natural graphite (ENG) to MOF-5 is a promising approach to improve the thermal conductivity by a factor of 5 [6,14]

To identify the potential of the synthesized hybrid monoliths for adiabatic adsorption processes, thermal and electrical properties have been evaluated. Table 2 reports the thermal conductivity measured for the different monoliths evaluated. The thermal performance of the pure MOF is very poor with a conductivity as low as $ca.$ 0.49 W m^{-1}K^{-1}, thus confirming the thermal insulating properties of MOFs (conductivities below 2 W m^{-1}K^{-1} at room temperature). As expected for a poly-crystalline sample, the reported value is slightly lower than the thermal conductivity measured for the HKUST-1 single crystal (0.69 W m^{-1}K^{-1}) [13]. Similar values have been reported in the literature for other MOF powders, such as IRMOF-1 (0.32 W m^{-1}K^{-1}), ZIF-8 (0.32 W m^{-1}K^{-1}), and HKUST-1 (0.26 W m^{-1}K^{-1}) [28—30]. Recent studies from Babaei et al. have anticipated that the thermal conductivity highly depends not only on the structure and composition of the MOF but also on the presence of remaining adsorbed molecules (e.g., solvent) in the network [13]. To mitigate these effects, samples were thermally treated before the conductivity measurements. According to Table 2, small contents of graphite flakes (10 wt%) incorporated does not modify the thermal performance. Only composites with 25 wt% and above give rise to a significant increase in the thermal transport properties (thermal conductivity values above 1—3 W m^{-1}K^{-1}). The limiting case corresponds to the pure graphite monolith with a thermal conductivity above 14 W m^{-1}K^{-1}.

HKUST-1@GF monoliths have also been tested in terms of electrical conductivity. Interestingly, the electrical conductivity is more sensitive to the chemical composition of the hybrid materials. While pure MOF exhibits infinite resistivity, i.e. the electrical conductivity is rather zero, the incorporation of graphite flakes gives rise to significant changes even at low concentrations. The higher sensitivity of the electrical conductivity vs thermal conductivity upon graphite incorporation must be associated with the different propagation mechanism (electron mobility towards phonon propagation) in both constituents of the monolith, i.e., graphite and MOF. Electrical conductivity in graphite is attributed to delocalized Π electrons, while thermal conductivity is attributed to lattice waves. Scattering of electrons and waves at the crystalline boundaries or atomic imperfections explain the thermal and electrical performance of graphites [31]. Concerning MOFs, the presence of cavities or pores and adsorbed molecules reduce the thermal conductivity due to the scattering of the framework phonons [13].

At this point it is important to highlight the large electrical conductivity achieved with the graphite flake monolith (above 1.1·10^4 S m^{-1}). This value is an average between the electrical conductivity of graphite in the parallel ($ca.$ 3·10^5 S m^{-1}) and perpendicular ($ca.$ 3.3·10^2 S m^{-1}) directions to the basal plane, thus confirming the random orientation of the microdomains in the monolith and the proper compaction achieved at the applied pressures [32].

To further evaluate the response of the monoliths under a thermal event (e.g., a massive adsorption process), heat dissipation processes have been evaluated in the different monoliths after irradiation with a NIR laser. To this end, two different experiments have been designed: i) direct NIR laser irradiation of the monoliths (808 nm wavelength and 0.6 W cm^{-2} power irradiation) and ii) thermal heating of the samples deposited on a ceramic surface pre-heated to 90 °C. The main goal was to evaluate the thermal response of the monoliths upon a thermal event and the subsequent cooling step. In both approaches, a thermographic camera was used to measure the temperature of the monoliths as a function of time during heating and cooling process.

Fig. 5a depicts the heating-cooling curves for samples $mono$-HKUST-1; $mono$HKUST-1@10GF; $mono$HKUST-1@25GF and mon-oHKUST-1@50GF. The graphite sample ($mono$GF) is not included

Table 2 — Thermal and electrical properties measured at 25 °C for the synthesized monoliths (experimental errors at 95% confidence are included).

Sample	Thermal properties	Electrical Properties	
	Conductivity (W·m^{-1}K^{-1})	Resistivity (Ω·m)	Conductivity (S·m^{-1})
$mono$HKUST-1	0.489 ± 0.004	∞	0
$mono$HKUST-1@10GF	0.500 ± 0.006	0.02381	42 ± 4
$mono$HKUST-1@25GF	1.06 ± 0.02	0.01250	80 ± 8
$mono$HKUST-1@50GF	3.15 ± 0.05	0.00124	805 ± 48
$mono$GF	14.2 ± 0.6	0.00009	11,345 ± 1050
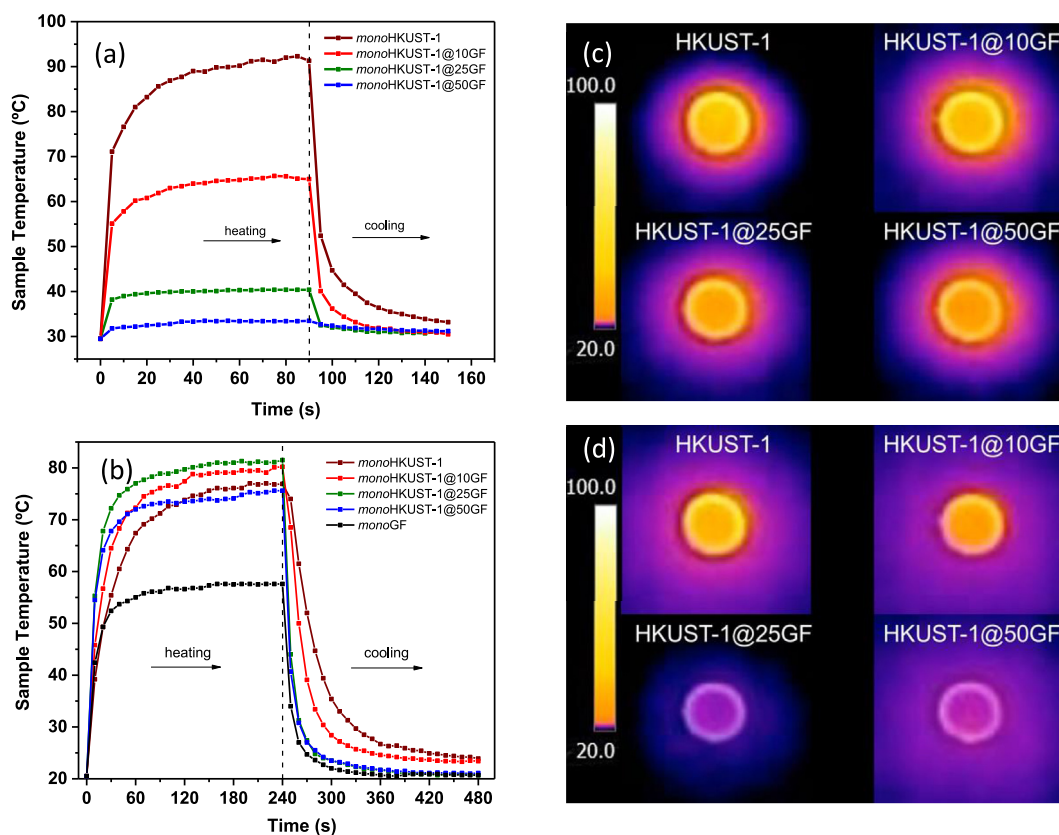
Fig. 5 — (a) Heating-cooling curves for samples *mono*HKUST-1; *mono*HKUST-1@10GF; *mono*HKUST-1@25GF and *mono*HKUST-1@50GF upon irradiation with NIR laser irradiation (808 nm wavelength and 0.6 W cm^{-2} of power irradiation), (b) Heating-cooling curves upon thermal heating on a ceramic surface at 90 °C, (c—d) Snapshots of the thermogravimetric camera in the cooling process at (c) t = 0 and (d) t = 10 s (complete video is provided as a complementary material).

here because the NIR laser irradiation conditions does not produce an appreciable temperature increase for this sample.

In the first approach, one can take advantage of the photothermal effect to induce local sample heating, and more specifically about the thermal effects after excitation of the Cu clusters (d-d transitions of the Cu(II) in the paddle wheels) [33]. The NIR laser source creates a heating spot of around 3 mm diameter in the surface of 13 mm diameter monoliths. The measured temperatures correspond to the whole monolith surface. The samples were irradiated during 90 s and then they were allowed to cool down (Fig. 5a). These experiments reflect clear differences in the temperatures reached by the samples after NIR irradiation. While HKUST-1 sample reaches the highest temperature of *ca.* 92 °C, the incorporation of graphite flakes in the composites greatly reduces the maximum temperature reached down to ~65 °C for *mono*HKUST-1@10GF, ~40 °C for *mono*HKUST-1@25GF and ~33 °C for *mono*HKUST-1@50GF. Notably, the NIR light irradiation did not give rise to any temperature increase in the graphite monolith. After irradiation, samples were cooled down in less than 60 s, this cooling being faster for monoliths with a larger amount of graphite in the formulation. However, the comparison among samples is not straightforward since the starting point (initial temperature) was different for each of the samples evaluated. In any case, these results anticipate that the incorporation of graphite flakes in the formulation of

the HKUST-1 monoliths increases the thermal conductivity of the monoliths, leading to a more efficient heat dissipation of the local photothermal heating generated within the monoliths upon irradiation for 90 s.

To evaluate the monoliths under similar thermal conditions, in a second approach the monoliths were exposed to a ceramic surface previously thermally treated at 90 °C. Fig. 5b depicts the heating-cooling curves for the different monoliths, including the pure graphite monolith. As described in the experimental section, the ceramic plate was heated at 90 °C during 240s and the different monoliths were deposited on the hot surface until thermal equilibrium was reached. Afterwards, the laser was stopped and the monoliths were allowed to cool down during additional 240s. The measured temperatures correspond to the whole monolith surface (Fig. 5b—d). According to Fig. 5b, during the stabilization step all *mono*HKUST-1-based samples reach a temperature around 75.6—81.5 °C, except pure graphite flakes where temperature is limited to 57.6 °C. As expected, the time needed to reach thermal equilibrium decreases with the GF content in the monoliths. Focussing in the cooling step, experimental results show that samples with the largest content of GF exhibit an increased heat dissipation rate. For instance, sample *mono*HKUST-1@25GF is able to reduce the temperature more than 54.1 °C in 30s, while in the same time interval pure *mono*HKUST-1 only decreases 24.9 °C in temperature. Overall, these results confirm that the incorporation of graphite flakes

increases the thermal conductivity of the composites and, hence, heat dissipation rates, leading to a faster heating when the ceramic surface is heated up to 90 °C and to a faster cooling when the ceramic surface is at RT.

Cooling rates have been estimated from the cooling profiles using the Newton's cooling model. According to the model, the heat loss rate in a hot body is directly proportional to the difference in the temperatures between the body and its environment, following equation (1):

$$T = T_{env} + (T_{max} - T_{env}) \cdot e^{(-kt)} \qquad \text{equation 1}$$

where T is the temperature of the monolith surface at a given time; T_{env} is the temperature of the environment and T_{max} is the temperature at which the cooling process starts. Table 3 displays the cooling rates obtained for the different samples evaluated.

The obtained rate constant values support the observed cooling trend in Fig. 5b and in the thermographic images (Fig. 5c&d) and videos (complementary material). These results confirm that samples monoHKUST-1@25GF, monoHKUST-1@50GF and monoHKUST-1@10GF have the highest dissipation rate. In other words, these results anticipate that 25 wt% of graphite is the minimum content in HKUST-1 monoliths to behave like pure graphite, in terms of heat dissipation rate (i.e., to have proper contact between graphite microdomains in the monolith).

Hydrogen adsorption performance

Although hydrogen storage in a potential application (e.g., transportation sector) is traditionally considered at cryogenic temperatures (−195 °C or above) and high pressures (ca. 10 MPa), changes in the inner porous structure of the sorbent (e.g., MOF) will be more clearly reflected in the low relative pressure range, when micropore have a major contribution. Fig. 6 clearly reflects that in powder form (left) pure HKUST-1 is the best performing sample with an excess (and total) uptake of 2.3 wt% [21]. Incorporation of graphite flakes (non-contributing to the adsorption performance) gives rise to a significant reduction in the total uptake down to 2.0 wt%, 1.4 wt% and 1.0 wt% for samples with 10, 25 and 50 wt% GF, respectively. After the conforming step, the scenario changes completely. For monoliths, sample monoHKUST-1@10GF exhibits the best adsorption performance with a total uptake above 1.7 wt%, followed by monoHKUST-1@25GF and the pure MOF. These results confirm the promoting effect of GF in the preservation of the 3D network in HKUST-1 upon a conforming step and the improved adsorption performance of the composites with a low GF content. In any case, the isotherms are fully reversible and exhibit a proper working capacity, independently of the formulation evaluated and the final conformation (powder or monolith).

In a final step, the volumetric adsorption capacity has been estimated from the gravimetric uptake for the monoliths using the real density (geometric density) calculated from the obtained monoliths. Fig. 6c clearly shows that the synthesized monoliths with 10 wt% GF are able to reach up to 18.7 g/L at −195 °C and atmospheric pressure (0.1 MPa). The volumetric uptake reached with our monolithic HKUST-1 containing 10 wt % GF is much higher than the value achieved with the powder material (7−8 g/L), higher than the simulated uptake for powder and monolithic HKUST-1 (15.3 g/L), and slightly lower than the

Table 3 — Cooling rates and thermal management parameters obtained from the Newton's model.					
	*mono*HKUST-1	*mono*HKUST-1@10GF	*mono*HKUST-1@25GF	*mono*HKUST-1@50GF	*mono*GF
T_{max} (°C)[a]	76.9	80.2	81.5	75.6	57.6
T_{env}[a]	20.5	20.5	20.5	20.5	20.5
k (s^{-1})	$0.012 \pm 1 \cdot 10^{-3}$	$0.013 \pm 3 \cdot 10^{-4}$	$0.024 \pm 4 \cdot 10^{-3}$	$0.019 \pm 2 \cdot 10^{-3}$	$0.022 \pm 1 \cdot 10^{-3}$
[a] Temperatures are determined with an accuracy of ±2.0 °C.					
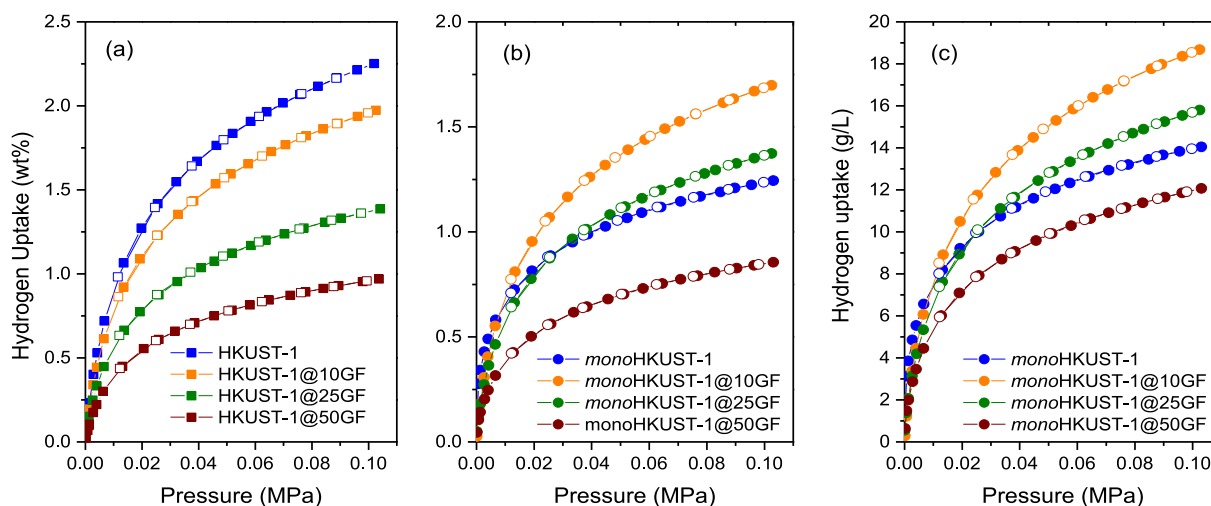
Fig. 6 — Hydrogen adsorption/desorption performance at −195 °C for the different composites in (a) powder and (b) monolithic form, both in gravimetric (a,b) and volumetric (c) basis.

best value reported in the literature for pure *mono*HKUST-1 (24 g/L), obtained using a completely different approach (sol-gel process) [10]. These values are also larger than those obtained with other MOFs in powder form at atmospheric pressure (MIL-53 Al, 5.2 g/L; MOF-5, 4.1 g/L; MOF-177, 3.4 g/L) [34]. Overall, these results confirm that high conductivity graphite flakes incorporated in the synthesis media for HKUST-1 constitute potential additives to i) infer "protection" of the MOF networks upon compaction, and ii) provide proper electrical and thermal properties, without significantly compromising the excellent adsorption properties of the parent MOF in powder form.

Conclusions

A series of HKUST-1 based samples modified with high conductivity graphite flakes (GF) have been synthesized using the conventional hydrothermal approach. Incorporation of GF to the synthesis media promotes the growth of high-quality MOF crystals with different morphologies. A subsequent conforming step at high pressure (377 kg/m^3) anticipates the promoting effect of the incorporated GFs in the protection of the embedded HKUST-1 crystals towards amorphization and/or plastic deformation. Furthermore, the presence of graphite microdomains in the formulation infers to the monoliths with excellent thermal and electrical properties. These properties are crucial for a fast and efficient dissipation of the adsorption heat generated in potential high storage tanks. Last but not least, the presence of GF in low concentration give rise to monoliths with excellent adsorption properties for hydrogen at cryogenic temperatures and atmospheric pressure, with values close to 19 g/L.

Declaration of competing interest

The authors declare that they have no known competing financial interests or personal relationships that could have appeared to influence the work reported in this paper.

Acknowledgements

Appendix A. Supplementary data

Supplementary data to this article can be found online at https://doi.org/10.1016/j.ijhydene.2023.05.357.

REFERENCES

[1] VijayaVenkataRaman S, Iniyan S, Goic R. A review of climate change, mitigation and adaptation. Renew Sustain Energy Rev 2012;16(1):878–97. https://doi.org/10.1016/j.rser.2011.09.009.

[2] Fan L, Tu Z, Chan SH. Recent development of hydrogen and fuel cell technologies: a review. Energy Rep 2021;7:8421–46. https://doi.org/10.1016/j.egyr.2021.08.003.

[3] Hirscher M, Yartys VA, Baricco M, Bellosta von Colbe J, Blanchard D, Bowman RC, Broom DP, Buckley CE, Chang F, Chen P, Cho YW, Crivello JC, Cuevas F, David WIF, de Jongh PE, Denys RV, Dornheim M, Felderhoff M, Filinchuk Y, Froudakis GE, Grant DM, Gray EMA, Hauback BC, He T, Humphries TD, Jensen TR, Kim S, Kojima Y, Latroche M, Li HW, Lototskyy MV, Makepeace JW, Møller KT, Naheed L, Ngene P, Noréus D, Nygård MM, Orimo S ichi, Paskevicius M, Pasquini L, Ravnsbæk DB, Veronica Sofianos M, Udovic TJ, Vegge T, Walker GS, Webb CJ, Weidenthaler C, Zlotea C. Materials for hydrogen-based energy storage – past, recent progress and future outlook. J Alloys Compd 2020;827:153548. https://doi.org/10.1016/j.jallcom.2019.153548.

[4] Suh MP, Park HJ, Prasad TK, Lim DW. Hydrogen storage in metal organic frameworks. Chem Rev 2012;112(2):782–835. https://doi.org/10.1021/cr200274s.

[5] Hirscher M, Panella B. Hydrogen storage in metal-organic frameworks. Scripta Mater 2007;56(10):809–12. https://doi.org/10.1016/j.scriptamat.2007.01.005.

[6] Purewal J, Liu D, Sudik A, Veenstra M, Yang J, Maurer S, Müller U, Siegel DJ. Improved hydrogen storage and thermal conductivity in high-density MOF-5 composites. J Phys Chem C 2012;116(38):20199–212. https://doi.org/10.1021/jp305524f.

[7] Peng Y, Krungleviciute V, Eryazici I, Hupp JT, Farha OK, Yildirim T. Methane storage in metal – organic frameworks: current records, surprise findings, and challenges. J Am Chem Soc 2013;135(32):11887–94. https://doi.org/10.1021/ja4045289.

[8] Tian T, Zeng Z, Vulpe D, Casco ME, Divitini G, Midgley PA, Silvestre-Albero J, Tan JC, Moghadam PZ, Fairen-Jimenez D. A sol-gel monolithic metal-organic framework with enhanced methane uptake. Nat Mater 2018;17(2):174–9. https://doi.org/10.1038/NMAT5050.

[9] Connolly BM, Aragones-Anglada M, Gandara-Loe J, Danaf NA, Lamb DC, Mehta JP, Vulpe D, Wuttke S, Silvestre-Albero J, Moghadam PZ, Wheatley AEH, Fairen-Jimenez D. Tuning porosity in macroscopic monolithic metal-organic frameworks for exceptional natural gas storage. Nat Commun 2019;10(1):2345. https://doi.org/10.1038/s41467-019-10185-1.

[10] Madden DG, O'Nolan D, Rampal N, Babu R, Çamur C, Al Shakhs AN, Zhang SY, Rance GA, Perez J, Maria Casati N Pietro, Cuadrado-Collados C, O'Sullivan D, Rice NP, Gennett T, Parilla P, Shulda S, Hurst KE, Stavila V, Allendorf MD, Silvestre-Albero J, Forse AC, Champness NR, Chapman KW, Fairen-Jimenez D. Densified HKUST-1 monoliths as a route to high volumetric and gravimetric hydrogen storage capacity. J Am Chem Soc 2022;144(30):13729–39. https://doi.org/10.1021/jacs.2c04608.

[11] Beckner M, Dailly A. A pilot study of activated carbon and metal-organic frameworks for methane storage. Appl Energy 2016;162:506–14. https://doi.org/10.1016/j.apenergy.2015.10.110.

[12] Grande CA, Vistad Ø. Adequacy versus complexity of mathematical models for engineering an adsorbed natural gas device. J Energy Storage 2020;28:101200. https://doi.org/10.1016/j.est.2020.101200.

[13] Babaei H, DeCoster ME, Jeong M, Hassan ZM, Islamoglu T, Baumgart H, McGaughey AJH, Redel E, Farha OK, Hopkins PE, Malen JA, Wilmer CE. Observation of reduced thermal conductivity in a metal-organic framework due to the presence of adsorbates. Nat Commun 2020;11(1):4010. https://doi.org/10.1038/s41467-020-17822-0.

[14] Liu D, Purewal JJ, Yang J, Sudik A, Maurer S, Mueller U, Ni J, Siegel DJ. MOF-5 composites exhibiting improved thermal conductivity. Int J Hydrogen Energy 2012;37(7):6109—17. https://doi.org/10.1016/j.ijhydene.2011.12.129.

[15] Huang BL, McGaughey AJH, Kaviany M. Thermal conductivity of metal-organic framework 5 (MOF-5): Part I. Molecular dynamics simulations. Int J Heat Mass Tran 2007;50(3—4):393—404. https://doi.org/10.1016/j.ijheatmasstransfer.2006.10.002.

[16] Casco ME, Fernández-Catalá J, Martínez-Escandell M, Rodríguez-Reinoso F, Ramos-Fernández EV, Silvestre-Albero J. Improved mechanical stability of HKUST-1 in confined nanospace. Chem Commun 2015;51(75):14191—4. https://doi.org/10.1039/c5cc05107j.

[17] Vishnyakov A, Ravikovitch PI, Neimark AV, Bülow M, Wang QM. Nanopore structure and sorption properties of Cu-BTC metal-organic framework. Nano Lett 2003;3(6):713—8. https://doi.org/10.1021/nl0341281.

[18] Chui SSY, Lo SMF, Charmant JPH, Orpen AG, Williams ID. A chemically functionalizable nanoporous material $[Cu_3(TMA)_2(H_2O)_3]_n$. Science 1999;283(5405):1148—50. https://doi.org/10.1126/science.283.5405.1148.

[19] da Silva CTP, Veregue FR, Moisés MP, Guilherme MR, Rinaldi AW. Synthesis of Al2O3-nanowhisker-based HKUST1 MOF composites. Mater Chem Phys 2019;232:446—51. https://doi.org/10.1016/j.matchemphys.2019.05.009.

[20] Zhang B, Huang P, Chen J, Dang X, Hu Y, Ai Y, Zheng D, Chen H. One-step controlled electrodeposition of iron-based binary metal organic nanocomposite. Appl Surf Sci 2020;504:144504. https://doi.org/10.1016/j.apsusc.2019.144504.

[21] Lin KS, Adhikari AK, Ku CN, Chiang CL, Kuo H. Synthesis and characterization of porous HKUST-1 metal organic frameworks for hydrogen storage. Int J Hydrogen Energy 2012;37(18):13865—71. https://doi.org/10.1016/j.ijhydene.2012.04.105.

[22] Zhang G, Wen M, Wang S, Chen J, Wang J. Insights into thermal reduction of the oxidized graphite from the electro-oxidation processing of nuclear graphite matrix. RSC Adv 2018;8(1):567—79. https://doi.org/10.1039/c7ra11578d.

[23] Wang Y, Lü Y, Zhan W, Xie Z, Kuang Q, Zheng L. Synthesis of porous Cu2O/CuO cages using Cu-based metal-organic frameworks as templates and their gas-sensing properties. J Mater Chem A 2015;3(24):12796—803. https://doi.org/10.1039/c5ta01108f.

[24] Rattanaweeranon S, Limsuwan P, Thongpool V, Piriyawong V, Asanithi P. Influence of bulk graphite density on electrical conductivity. Procedia Eng 2012;32:1100—6. https://doi.org/10.1016/j.proeng.2012.02.061.

[25] Sakanaka Y, Hiraide S, Tanaka H, Hiratsuka T, Kojima N, Yamane Y, Miyahara MT. Efficiency of thermal management using phase-change material for nonisothermal adsorption process. Ind Eng Chem Res 2020;59(32):14485—95. https://doi.org/10.1021/acs.iecr.0c02344.

[26] Gautam, Sahoo S. Thermal management and optimization of adsorption vessels for CO2-based green refrigeration systems: a heat and mass transfer approach. Sadhana - Acad Proc Eng Sci 2021;46(4):1—21. https://doi.org/10.1007/s12046-021-01774-2.

[27] Wieme J, Vandenbrande S, Lamaire A, Kapil V, Vanduyfhuys L, Van Speybroeck V. Thermal engineering of metal-organic frameworks for adsorption applications: a molecular simulation perspective. ACS Appl Mater Interfaces 2019;11(42):38697—707. https://doi.org/10.1021/acsami.9b12533.

[28] Huang BL, Ni Z, Millward A, McGaughey AJH, Uher C, Kaviany M, Yaghi O. Thermal conductivity of a metal-organic framework (MOF-5): Part II. Measurement. Int J Heat Mass Tran 2007;50(3—4):405—11. https://doi.org/10.1016/j.ijheatmasstransfer.2006.10.001.

[29] Cui B, Audu CO, Liao Y, Nguyen ST, Farha OK, Hupp JT, Grayson M. Thermal conductivity of ZIF-8 thin-film under ambient gas pressure. ACS Appl Mater Interfaces 2017;9(34):28139—43. https://doi.org/10.1021/acsami.7b06662.

[30] Chae J, An S, Ramer G, Stavila V, Holland G, Yoon Y, Talin AA, Allendorf M, Aksyuk VA, Centrone A. Nanophotonic atomic force microscope transducers enable chemical composition and thermal conductivity measurements at the nanoscale. Nano Lett 2017;17(9):5587—94. https://doi.org/10.1021/acs.nanolett.7b02404.

[31] Tyler WW, Wilson Jr AC. Thermal conductivity, electrical resistivity and thermoelectric power of graphite. Phys Rev 1953;89(4):870—5. https://doi.org/10.1103/physrev.89.870.

[32] Deprez N, McLachlan DS. The analysis of the electrical conductivity of graphite conductivity of graphite powders during compaction. J Phys D Appl Phys 1988;21(1):101—7. https://doi.org/10.1088/0022-3727/21/1/015.

[33] Espín J, Garzón-Tovar L, Carné-Sánchez A, Imaz I, Maspoch D. Photothermal activation of metal-organic frameworks using a UV-vis light source. ACS Appl Mater Interfaces 2018;10(11):9555—62. https://doi.org/10.1021/acsami.8b00557.

[34] Ramirez-Vidal P, Canevesi RLS, Celzard A, Fierro V. Modeling high-pressure hydrogen uptake by nanoporous metal—organic frameworks: implications for hydrogen storage and delivery. ACS Appl Nano Mater 2022;5(1):759—73. https://doi.org/10.1021/acsanm.1c03493.